ICAS-88-4.9.1

EXPERIMENTAL INVESTIGATION OF THE COMPLEX 3-D FLOW AROUND A BODY OF REVOLUTION AT INCIDENCE. A SINO-ITALIAN COOPERATIVE RESEARCH PROGRAM *

G. Iuso; M. Onorato - Aeronautical and Space Dept., Politecnico di Torino, Torino (Italy)

M.S. Oggiano - Fluidynamics Research Centre of CNR, Politecnico, Torino (Italy)

S. De Ponte - Aerospace Dept.,Politecnico di Milano, Milano (Italy)

Bian Yuzhong; Zhang Xiaodi - Harbin Aerodynamics Research Institute, Harbin (China)

Abstract

In this paper some significant results obtained during a cooperative research program between the Chinese Aeronautical Establishment, some Italian Universities and the "Centro Studi Dinamica Fluidi" of C.N.R. are shown. The research program is about the experimental study of the 3-D complex flow around a prolate ellipsoid at angle of attack. Many different tests have been carried out in different wind tunnels in China and in Italy: flow visualizations, pressure and force measurements, boundary layer surveis and LDV measurements.

The results are discussed trying to give a physical picture of the complex flow around the model.

I. Introduction

Since 1984 cooperative research programs in the field of Aeronautics were established between the Chinese Aeronautical Establishment (C.A.E.) and some Italian Universities under the auspices of the Chinese Ministry of Aviation and the Italian Foreign Affair Office.

One of these programs, dealing with the experimental investigation of the complex 3-D incompressible flows around bodies having simple geometrical characteristics, has been already completed.

The aim of this paper is to show some significant results that have been obtained.

The body under investigation has been an axi-symmetric ellipsoid having the axis ratio of 6:1, that has been tested at different angles of attack. The reasons of chosing this body are its simple geometrical shape, and the fact that a similar model was under investigation at the DFVLR Institute of Experimental Fluid Mechanics in Goettingen[1,2,3]. Moreover the flow field around this ellipsoidal shaped body posses all the relevant features of the flow around bodies of practical interest, as fuselages, missiles and ship hulls.

The aims of this study are various:

- Complex fluidynamical phenomena like 3-D transition from laminar to turbulent flow, 3-D flow separation, viscous-inviscid flows interactions around bodies of revolution are far to be completely understood. An attempt to give a clearer physical picture of such phenomena is one of the main goal.

- The state of the art of the computational fluidynamics is at the mature stage to be confidently used for engineering applications, but still its use relies upon some empirical assumptions. Three-dimensional boundary layer codes assume velocity profile shapes, entrainment rate and skin friction law if integral methods are used; they assume turbulence models if field methods are used. Relatively few experimental results are available to describe with confidence averaged quantities and very few to model turbulence. Most turbulence models are straightforward extensions of existing two-dimensional models. It is not well know the influence of streamline convergence and divergence and the influence of streamline curvature on turbulence properties. Also it is not clear how the skewed mean velocity profile distorts the structure of the large eddies. As a consequence, numerical codes must be calibrated and validated before applied to real problems. The aims of this study is also that of producing data for calibration and validation.

The tests were performed in three different wind tunnels at the Harbin Aerodynamics Research Institute of C.A.E.[4] and at the "M. Panetti" Aerodynamics Laboratory of the Politecnico di Torino[5]. The experiments consisted on:

1. - surface shear stress visualizations by oil flow method
2. - flowfield visualization by color helium bubble technique
3. - flowfield visualization by total pressure probe color picture technique
4. - body forces and moments measurements
5. - surface pressure distribution measurements
6. - surface shear stress measurements by pressure wall skin friction probes
7. - boundary layer velocity profiles measurements by pressure probes and by hot wire probes
8. - distribution of longitudinal and vertical velocities at the lee side of the model, for high angle of attack, by a two colors laser doppler velocimeter

Measurements cover a large range of angle of attack, from 0^o to 30^o, including different flow field conditions from fully axisymmetric attached flow to heavily 3-D separated flow. Experiments have been performed with free and artificial transition and at different Reynolds numbers.

Due to the fact that it is not possible to report all results in a single paper, a panoramic view of the flow fields, mainly based on flow visualizations and forces measurements, for different angles of attack is given, while boundary layer results are shown only for an intermediate angle of attack, $\alpha = 14^o$.

The last choice follows from the consideration that at such angle of incidence most of the features typical of 3-D separated flows around axi-symmetric bodies are present, but still the viscous-inviscid interaction may be considered not strong such that the flow field may be modelled by zonal methods.

LDV measurements, due to their unique feature to describe complex flows, are shown for an high angle of attack, $\alpha = 30^o$.

- (*) The italian part of this research has been supported by M.P.I. (Ministry of Education of Italy) and by C.N.R. (National Council of Research of Italy)

II. Wind Tunnels and Model

Experiments have been performed in three different wind tunnels. Force measurements have been carried out in the 3.5m by 2.5m, closed test section, low speed wind tunnel of C.A.E. of Harbin. Surface and flow field visualizations and LDV measurements have been performed in the 1.5m diameter, open test section, low speed wind tunnel of C.A.E. of Harbin. Surface pressure distribution measurements, surface shear stress visualizations, surface shear stress measurements, 3-D boundary layer velocity surveys have been carried out in the 3m diameter, closed test section wind tunnel of Politecnico di Torino.

Unfortunately, the tests in the three tunnels are complementary and not direct comparison of the same results obtained in the different tunnels are available. Probably this could be matter for a future join research project; the three tunnels have comparable dimensions and speed range, and different free stream turbulence intensity and structure and it could be of great interest to correlate results mainly regarding transition location from laminar to turbulent flow and surface shear stress in the fully developed turbulent boundary layer.

Different models have been used according to the different tests. They all have been manufactured using the same mould and are made of two half-shells of glass fiber reinforced resin with a wall thickness of 5mm, the major and minor axis are respectively of 1.5m and 0.25m.

The models were mounted in the wind tunnel test section by means of an axial sting which could be rotated around the body axis by a stepper motor device with steps of 0.02° (Fig.1). In this way it was possible to locate a limited number of pressure holes and probes on the body along meridians, while the measuring points could be selected with large freedom in circumferential position.

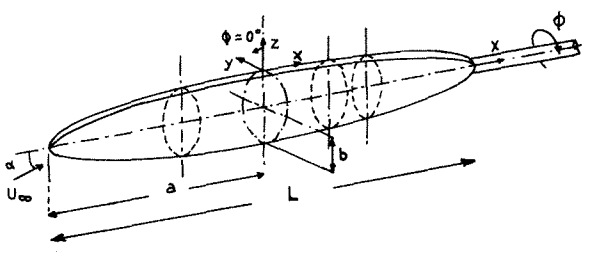

Fig.1 - Ellipsoid model and coordinate system.

It is well known that in some cases the asymmetry of the flow around bodies of revulution is triggered by some nose imperfection and the flow swithches from one side to another while rotating the model. It is a risk which cannot be avoided when it is necessary to use a limited number of probes. In any case, up to now all the measurements have not shown this kind of switching instability: careful checks were made to detect any of these phenomena.

In the tests with imposed transition, a sandpaper strip, 20 mm width and 0.7mm grain diameter, was located at 20% of the major axis from the nose.

The model for surface pressure and shear stress measurements and for boundary layer survey were inside equipped with a Scanivalve system and 4 transversing mechanism allowing displacement of miniature probes in the perpendicular direction relative to the model surface. The model for force and moment measurements was equipped with an internal balance. The model for surface flow visualization was free of pressure taps.

III. Experimental Technique and Results

The visualization of surface shear stress has been performed by painting the model by a mixture of oil and white powder. The surface flow pattern found after the run gives informations about the off-surface flow structure. Tests have been runned at a speed of 30 m/s, for α ranging from 0° to 30°.

Examples of results are shown in Fig.2, for the case of free transition.

Flow field visualizations have been accomplished by a color helium bubble technique, that has been developed at Harbin C.A.E. Laboratory[6]. The helium bubble generator can move through the field in order to observe global and local flows. Visualized stream lines are recorded by photographic camera. Flow field visualizations have been performed at a stream velocity of 10 m/s and angle of incidence varying from 0° to 30°.

Few results are here reported in Fig.3, for the case of free transition; unfortunately not all the informations from the visualizations appear from the pictures, due to their reproduction in black and white.

Flow field visualizations in planes orthogonal to the main flow direction have been accomplished by total pressure probe color picture technique. A pitot probe fixed on a traversing mechanism external to the model may perform complete survey of a given portion of plane, detecting the level of the local total pressure. The pressure variations given by voltage signals were transformed into different color signals by an electric-optic transform system and were retransmitted through optic fiber into the tunnel for photographic recording. The colors display on the picture gives (quasi-quantitative) informations on the loss of total pressure of the flow. Minimum allowed distance between the probe and the model was about 5mm. Experiments were performed at an upstream velocity of 35 m/s, for α varying from 0° to 30°. Few examples are shown in Figs.4, for the case of free transition.

Also in this case, due to the black and white reproduction in this paper, the informations given by the pictures does not appear in their completeness.

Global measurements of forces and moments acting on the model were performed by an internal six components balance, for α varying from 0° to 30° and stream velocities from 10 m/s to 40 m/s.

Results are displayed in Fig.5, for the case of free transition.

Surface pressure distributions were measured by means of 72 pressure taps:40 of them are located along an ellipsoid meridian, some of the other were located on other meridiansto check the flow stability with respect to the switching of asymmetries. Measurememts were taken rotating the model around its axis by steps of 18°,for flow velocities from 10 m/s to 40 m/s and α ranging from 0° to 45°.

In Figs.6a and 6b results for different values of α are shown, for the case of free transition. Fig.6c refers to the case of fixed transition.

Skin friction measurements were performed by 2-dimensional wall pressure type miniature probes, located along a helix on the body, in order to minimize interference. Ten of such probes are positioned along the model as indicated in Table I.

The probes consist of two joint flattened tubes, acting as pair of Preston tubes, with their axis parallel to the meridian direction and with the frontal- holes cut normally to the model surface with their planes at angles of respectively $+45°$ and $-45°$ with respect to the ellipsoid meridian. Aside of each of the probes there are two wall pressure taps, to give an interpolated local wall pressure value. The three readings, the left and right tube

holes pressures and the wall pressure, going through a complex interpolation procedure with a set of calibration curves, give the direction of the wall shear stress and give the value of an equivalent Preston tube pressure; from this the value of the skin friction is obtained by means of a classical Preston tube calibration diagram.

TABLE I

shear stress probes	x mm	Ø
1	208.5	200°
2	334.5	215°
3	463.5	230°
4	592.5	245°
5	739.5	260°
6	847.5	275°
7	978.0	290°
8	1107.0	305°
9	1237.5	320°
10	1324.5	335°

In Fig.7 a shear stress polar plot, for $\alpha = 14^o$ and $Re = 3 \times 10^6 (V_\infty = 30m/s)$ is shown, for the case of fixed transition. Three dimensional velocity profiles measurements were carried out by two types of pressure probes: a standard wedge, flattened tubes, 2-holes probe and a 3- holes probe. The first were used in sections were no separation was expected from the pressure measurements and from the flow visualization. In this case it was reasonable to assume rather constant static pressure across the boundary layer and insignificant values of the velocity component normal to the wall. The second was used downstream, near regions of flow separation, triying to measure the normal velocity component. Aside of each probe there are two wall pressure taps, to interpolate the local wall pressure. The probes were calibrated to give flow direction and flow velocity, when positioned with their axis parallel to the body meridian. The transversing mechanisms, inside the model, operated by a DC motor and monitored by a potentiometer, were controlled via an adequate hardware by a small data acquisition computer. The resultant displacement resolution was 0.02mm. Four of such probes were positioned on the model at the points reported in Table II.

TABLE II

velocity profiles probes	x mm	Ø
1	463.5	91°
2	739.5	132°
3	978.0	150°
4	1107.0	174°

In Fig.8 boundary layer total and cross velocity profiles, for different cross sections and different values of the roll angle Φ are shown. The results refer to a Reynolds number of $Re = 3 \times 10^6 (V_\infty = 30m/s)$, $\alpha = 14^o$, and to the case of fixed transition. On the same figure values of the displacement thickness δ^*, the momentum thickness θ and the velocity profile shape factor $H = \delta^*/\theta$ are reported. Finally in Fig.9 the distribution of displacement thickness along the circumferential direction are displayed for different cross sections and same flow conditions as in Fig.8.

Laser Doppler velocimeter measurements were carried out using a TSI 91007 two colors equipment. Distributions of longitudinal and vertical velocities were measured at the lee side model in two sections,at a free stream velocity of 20 m/s and angle of attack $\alpha = 30^o$.

Results are shown in Figs. 10a and 10b, for the case of free transition.

IV. Analysis of the Results

An overall picture of the flow around the model, for increasing values of α, may be seen from the flow visualization results shown in figures 2,3 and 4. Oil flow gives a view of the surface shear stress directions and the found surface flow patterns determine the structures of the off-surface flow; this flow leaves the body and rolls up to form the leeward-side vortices along *surfaces of separation*. The surfaces of separation (vortex sheets) intersect the body surface along the lines of separation, easily visible on the pictures as the converging lines emanating from the saddle point of separation. Combining skin friction line patterns with field visualization by helium bubble technique, the flow behaviour may be understood more clearly.

For $\alpha = 10^o$ vortex flow appears near the tail region of the lee side of the model. Increasing the angle of attack to 15^o, separation line extends toward the nose of the body and also vortex flow region enlarge toward the nose; vortex flow appears near $x/2a = 0.8$. With increasing angle of attack, vortex region extends more and more upstream and for $\alpha = 30^o$ vortex sheets are already visible for $x/2a = 0.4$. Comparing figs 2 and 3 it should be noted that the Reynolds numbers for the two flow visualization are quite different.

The extension and the strenght of lee-ward side vortices may be observed by the total pressure color pictures. For each angle of attack flow surveis are reported in four different cross sections. For $\alpha = 10^o$, the picture at the section $x/2a = 0.625$ shows that a vortex region is forming, but still the flow may be considered attached. At the section $x/2a = 0.825$ two symmetrical vortices can be seen on the lee side of the model. Further downstream at $x/2a = 0.936$ and at $x/2a = 1.02$ the vortex region becomes more and more extensive and we observe a lack of symmetry. At the last station the left vortex height above the model surface is about 57mm and the right vortex height is about 42mm.

With increasing α to 15^o, similar flow behaviour may be found in correspondent cross sections, but with larger vortical flows and higher vortex strenght. The last can not be seen in the pictures due to the black and white reproduction.

The flow field appears much more complex at higher angle of attack, $\alpha = 30^o$, where flow separation and vortex formation are already evident at $x/2a = 0.309$ and the the vortex extension and the growth are such that the two controrotating vortices apparently merge going downstream. This effect may be explained observing that the color regions shown are regions of equal total pressure loss and not regions of equal vorticity.

The results of six components forces and moments balance measurements are shown in Fig.5 for different values of the upstream flow velocity and free transition. The coordinate system is the wind axis system and the reference point for the moment is the centroid of the model. Reference lenght is the minor ellipsoid axis and reference area is the model maximum cross-section.

Looking at the results, the lift coefficient shows the typical non linear slender body characteristics of vortex lift. The same happens for drag. It is interesting to observe the behaviour of

lift and drag at the lowest Reynolds number tested: their values are much higher than at 20 m/s, which in turn are lower than at higher velocities. This behaviour may be tentatively associated to the sequence of:

- laminar separation without close reattachement at the lee-side near the nose
- bubble type separation with turbulent reattachement and successive turbulent separation
- turbulent separation without reattachement as we increase the Reynolds number.

This is in line with the flow on spheres and cylinders and explains the sudden decrease of drag with Reynolds number and the successive reincrease.

The drop of pitching moment for the 10 m/s case is also conform with this possible flow behaviour. The drop could be explained as due to the absence of suction close to the nose, due to laminar separation. The pitching moment shows moreover the maximum Reynolds number effect.

To investigate the flow asymmetry, yet observed in the results from flow visualizations, it is interesting to observe side force, rolling and yawing moments. All three are very small and about constant up to 15° and the non zero values may be easily explained with some misalignement respect to the flow. Beyond that angle of attack, the low Reynolds number case shows some random behaviour, probably due to transitional flow. Other cases display an asymmetry increasing with speed.

Details of pressure distributions are shown in figures 6a and 6b. In Fig.6a pressure coefficients, as function of the circumferential position, are displayed for three axial stations, corresponding to the nose and afterbody regions. In Fig.6b the pressure coefficient is reported along the upper meridiane, $\Phi = 0°$. The shown pressure distributions are characterized by large suctions area at the body sides. The suction maximum values are slightly shifted from the upper to lower part of the body, going downstream, due to the charge in position of the separation line, as it is shown from the flow visualization results. On the nose region the flow goes from stagnation conditions to a high suction peak, from which the pressure increases rapidly going downstream.

In Fig.6c pressure distributions are shown for the conditions corresponding to the boundary layer measurements, for fixed transition and $\alpha = 14°$, $Re = 3 \times 10^6$.

Boundary layer results are reported in figures 7, 8 and 9, for the case of $\alpha = 14°$. The results from shear stress measurements are shown in Fig.7 under the form of vector plots. It is evident the location of separation lines from the convergence of the limiting streamlines. Separation lines appear at $x/L = 0.6$ and $\Phi = 40°$, and look symmetrical up to $x/L = 0.85$. Downstream on the afterbody, the shear stress field appears no longer symmetrical, although it is symmetrical before separation. This asymmetry is in accordance with flow visualization results and force measurements and generally in accordance with other observed instabilities in vortical flows[7].

Total velocity profiles and cross velocity profiles on the body are shown in Figs.8. On the windward side typical 2-D turbulent profiles may be seen; the aspect of profiles changes approaching separation. Along the leeward line, attached flow conditions are evident also in the afterbody region.

In Fig.9 displacement thickness distributions are plotted in the circumferential direction. An increase in thickness toward the separation region with a maximum corresponding to the minimum shear stress is observed. The boundary layer parameters, except in a region close to separation, approach the well known values which characterize simple turbulent boundary layer, as mainly pointed out by the constant shape factor parameter around the value of 1.3, which is typical of any 2-D accelerating boundary layer.

It means that, apart from the region which approaches the separated flow, the boundary layer has about two dimensional characteristics. Only for $x/L = 0.65$ and $\Phi = 240°$ the flow direction changes by 18° from the wall to the outer stream.

Finally results from Laser Doppler velocimeter are shown in Figs. 10a and 10b, where, respectively, longitudinal and vertical velocity distributions are displayed in function of the lateral distance y, for different heights z, at the lee side region of the model. Free stream velocity was 20 m/s and the angle of attack $\alpha = 30°$. Measurements were taken in two different cross sections corresponding to $x/2a = 0.480$ and $x/2a = 0.652$. At $x/2a = 0.480$ two vortex regions appear, vortices are not strong and are symmetric. Downstream, at $x/2a = 0.652$, the two vortex regions appear asymmetric as it is evident from both the longitudinal and vertical velocity distributions.

V. Conclusions

- Results obtained during a cooperative research program between the C.A.E., some italian Universities and the "Centro Studi sulla Dinamica dei Fluidi" of C.N.R. have been shown.
- The combination of surface and field visualizations and measurements has given a contribution to a better physical knowledge of the complex 3-D flow around a model of prolate ellipsoid at angle of attack.
- For the case of $\alpha = 14°$, results from boundary layer measurements have been reported. At this angle of attack the main features of the 3-D flow around body of revolutions are present, but still the viscous inviscid interaction may be considered not strong. The data offered could be than of interest for 3-D boundary layer codes calibration and validation and to assest the procedures to take into account viscous-inviscid interactions. More data are available, that have been not reported here.

References

1. - H.U. Meier, H.P. Kreplin *Pressure distributions and flow visualizations on an ellipsoid 1:6 designed for 3-D boundary layer investigations.* Proc. 7th U.S. Air Force/Fed. Rep. Germany data exchange agreement meeting, Tech.Rep. (1978)

2. - H.U. Meier, H.P. Kreplin *Experimental investigation of the boundary layer transition and separation on a body of revolution.* Proc. of the 2th Symp. on Turbulent Shear Flows, Imperial College, London (1979)

3. - H.U. Meier, H.P. Kreplin, X. Ming *Problems associated with artificial boundary layer transition*AIAA 16th Fluid and Plasma Dynamics Conf. Danvers, USA (1983)

4. - B. Yuzhong, Z. Xiaodi *Experimental investigation of flow field about and forces on an ellipsoid shaped model.* CAE - HARI Internal Report (1986)

5. - G. Iuso, M.S. Oggiano, S. De Ponte, B. Yuzhong, Z. Xiaodi *3-D Boundary layer measurements on an ellipsoid at angle of attack.* Proc. of the ICFM, Beijing (1987)

6. - Z. Dong, W. Zhongqi, Z. Xiaodi, Q. Jialin, L. Xianzhong *Colour helium bubble flow visualkization technique.* Proc. of 15th ICAS, London (1986)

7. - P.Campigny *Reynolds number effect on the aerodynamic characteristics of an ogive-cylinder at high angles of attack.* AIAA 2nd Applied Aerodynamics Conf., Seattle (1984)

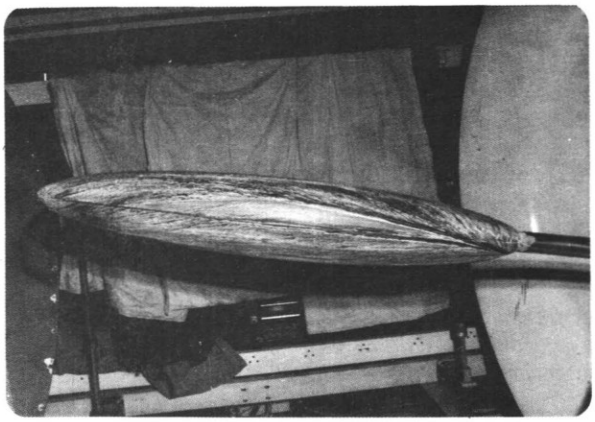

Fig.2 - Oil flow visualization. $\alpha = 10°$. Free transition.

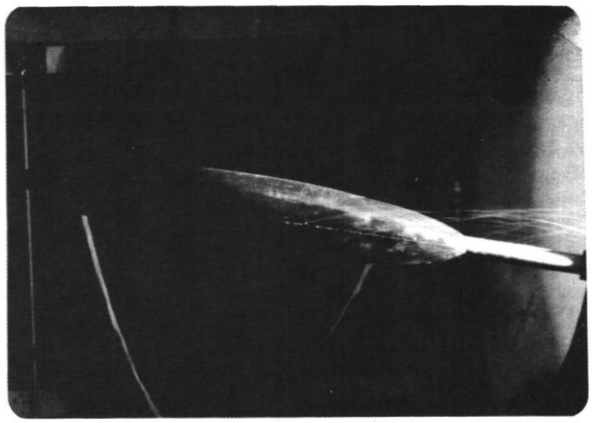

Fig.3 - Helium bubble flow visualization. $\alpha = 10°$. Free transition.

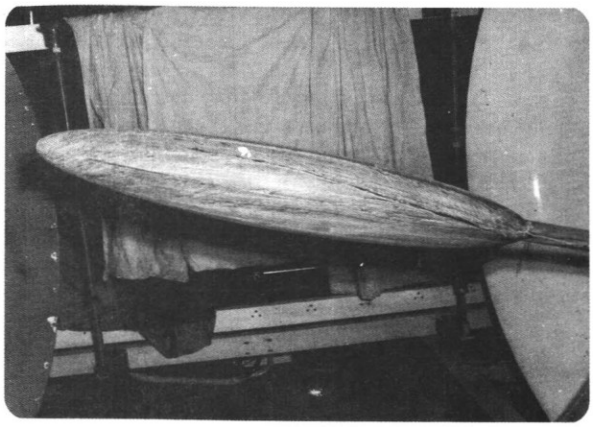

Fig.2 - Oil flow visualization. $\alpha = 15°$. Free transition.

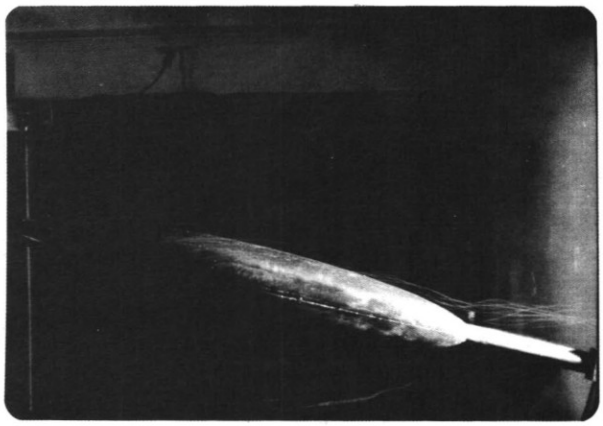

Fig.3 - Helium bubble flow visualization. $\alpha = 15°$. Free transition.

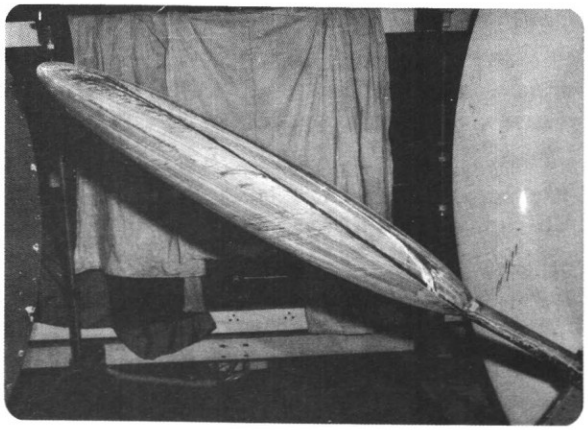

Fig.2 - Oil flow visualization. $\alpha = 30°$. Free transition.

Fig.3 - Helium bubble flow visualization. $\alpha = 30°$. Free transition.

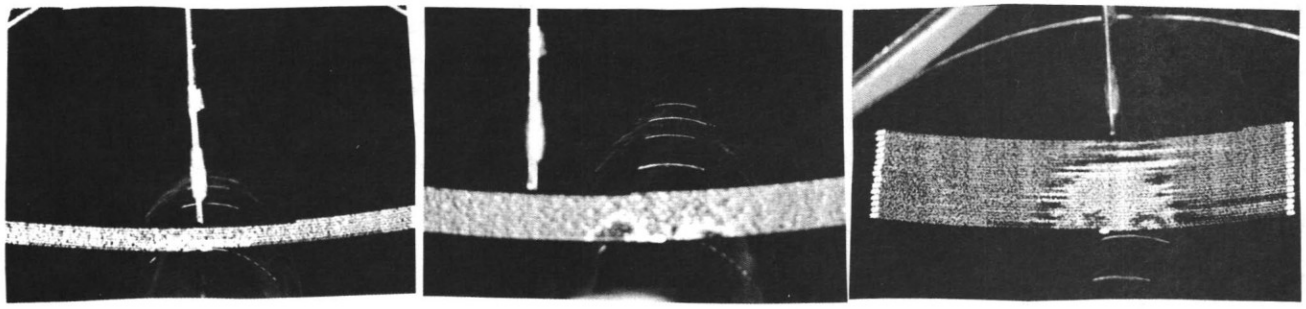

α = 10°, x/2a=.625 α = 15°, x/2a=.650 α = 30°, x/2a=.309

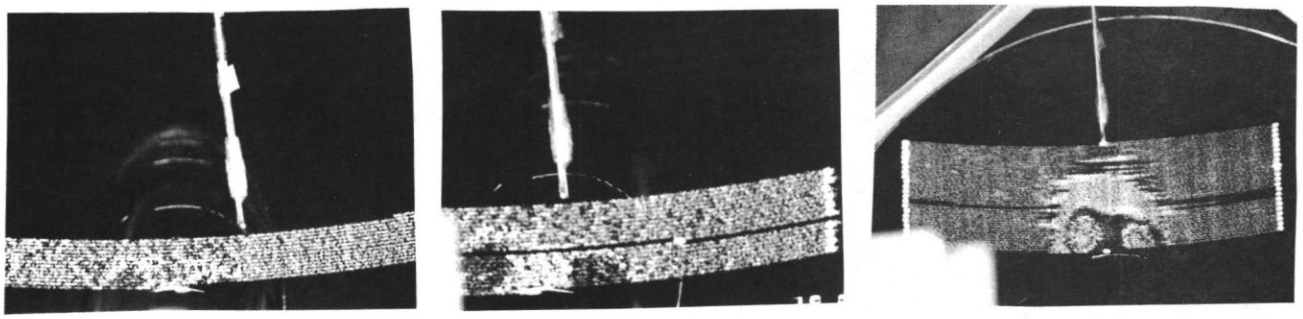

α = 10°, x/2a=.825 α = 15°, x/2a=.825 α = 30°, x/2a=.480

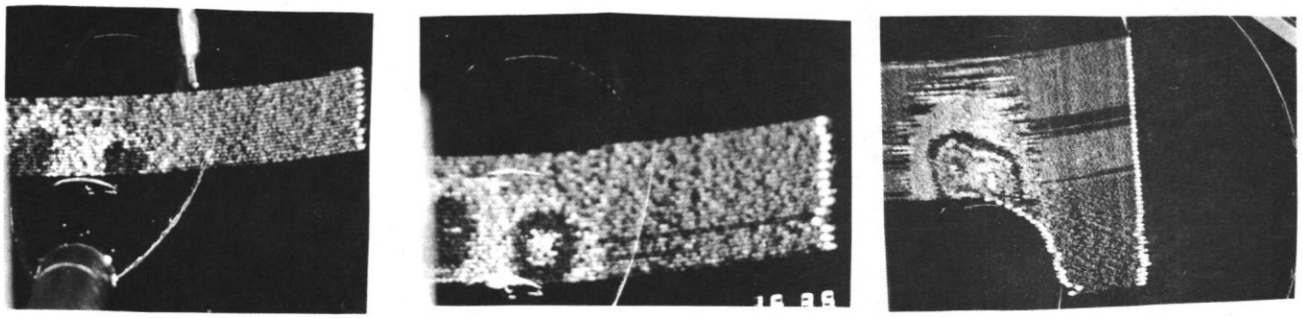

α = 10°, x/2a=.936 α = 15°, x/2a=.936 α = 30°, x/2a=.652

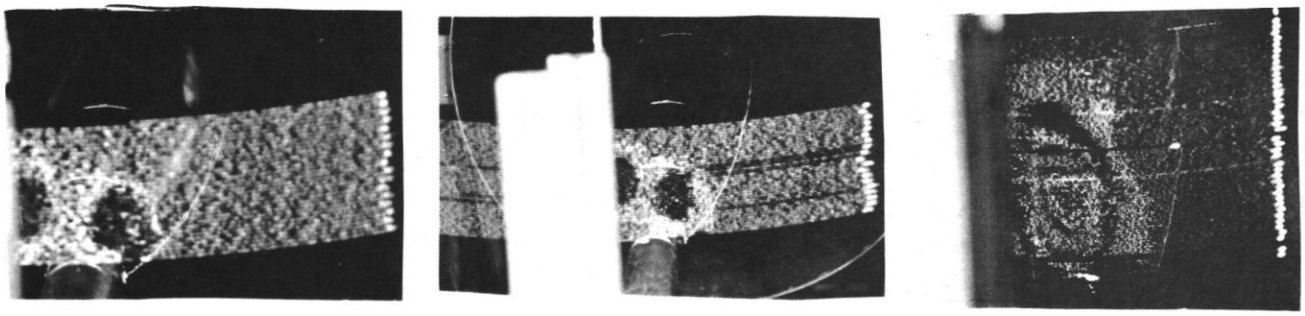

α = 10°, x/2a=1.02 α = 15°, x/2a=1.02 α = 30°,x/2a=.936

Fig.4 - Total pressure lost visualization. Free transition.

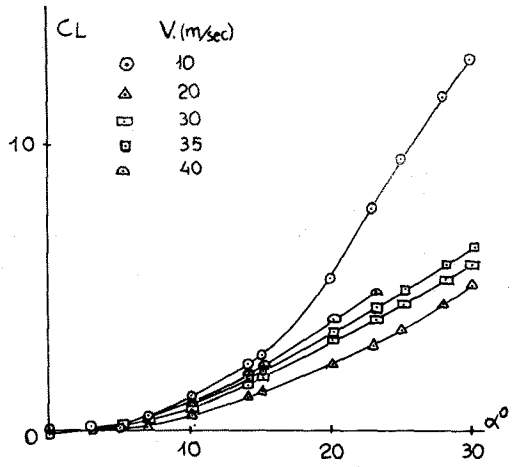

Fig.5 - Lift coefficient versus α. Free transition.

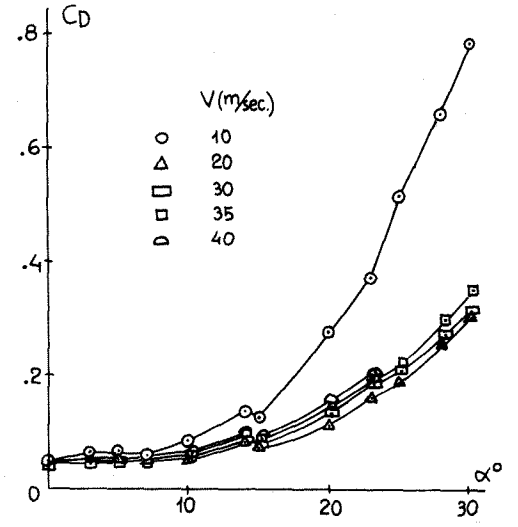

Fig.5 - Drag coefficient versus α. Free transition.

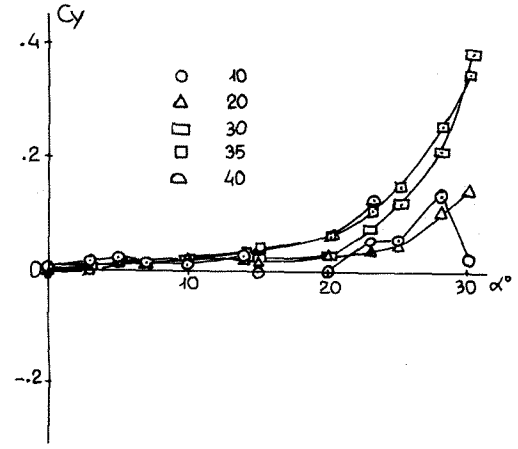

Fig.5 - Side force coefficient versus α. Free transition.

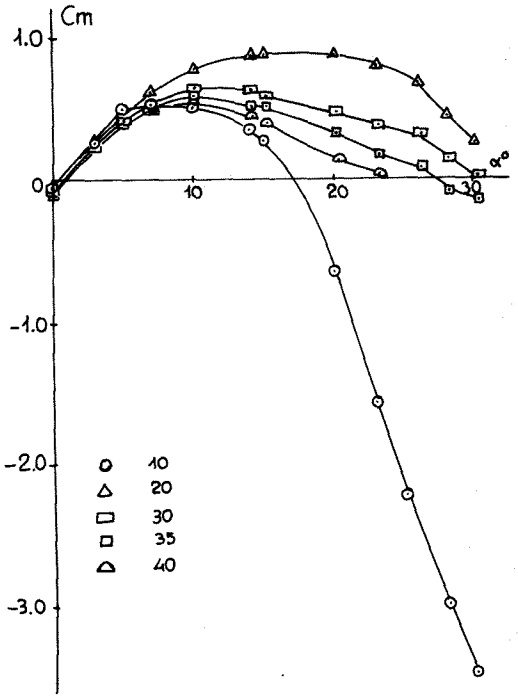

Fig.5 - Pitching moment versus α. Free transition.

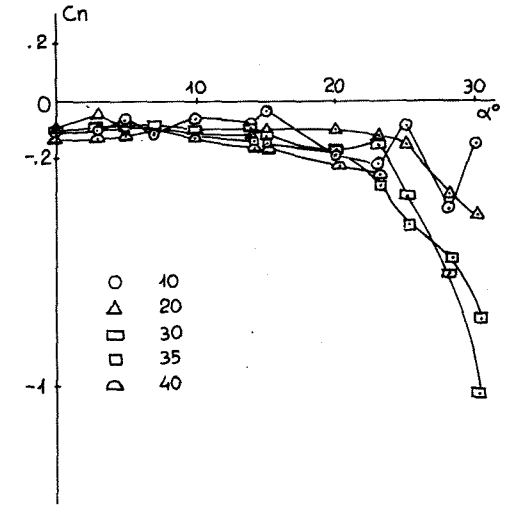

Fig.5 - Yawing moment versus α. Free transition.

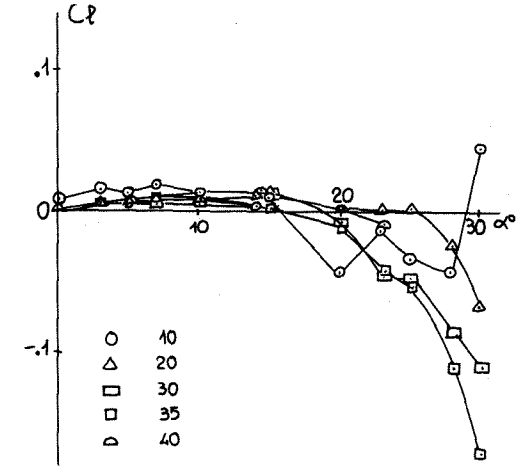

Fig.5 - Rolling moment versus α. Free transition.

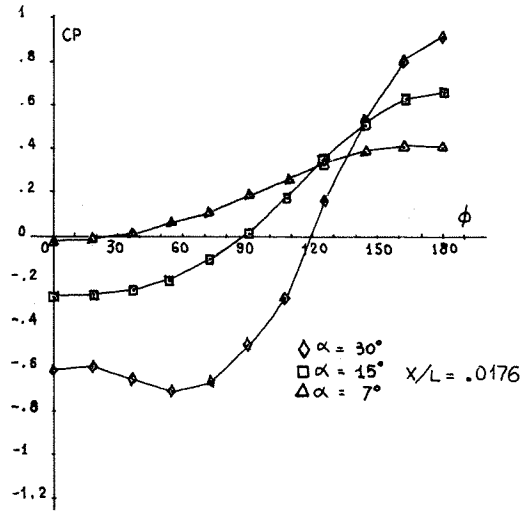

Fig.6a - Pressure distributions along a body parallel, at different angle of attack; ($V_\infty = 27m/s$), x/L = 0.0176, Free transition.

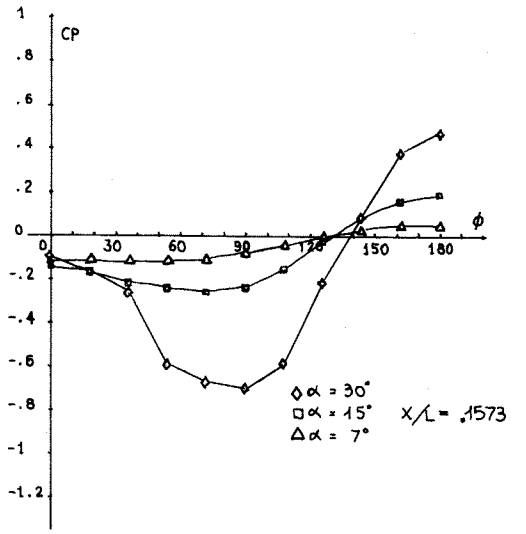

Fig.6a - Pressure distributions along a body parallel, at different angle of attack; ($V_\infty = 27m/s$), x/L = 0.1573, Free transition.

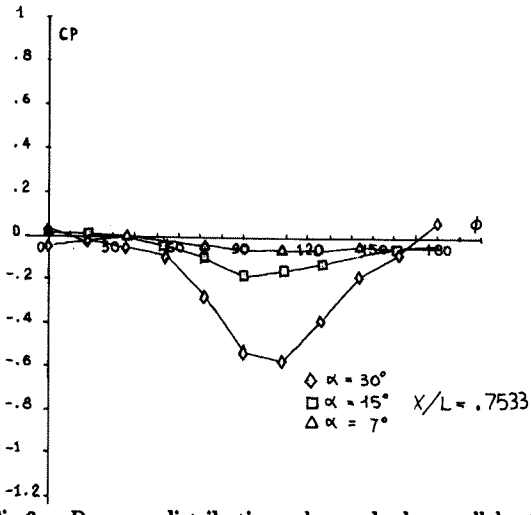

Fig.6a - Pressure distributions along a body parallel, at different angle of attack; ($V_\infty = 27m/s$), x/L = 0.7533. Free transition.

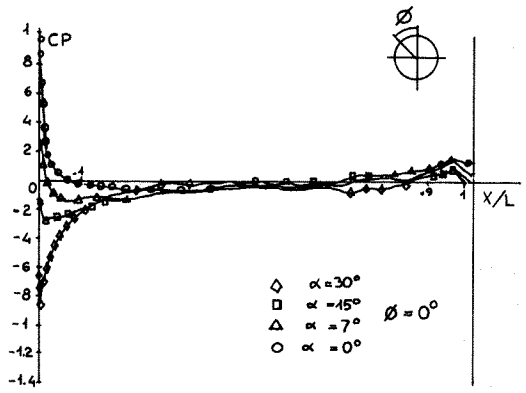

Fig.6b - Pressure distributions along the meridian, $\Phi = 0°$, at different angle of attack; ($V_\infty = 27m/s$). Free transition.

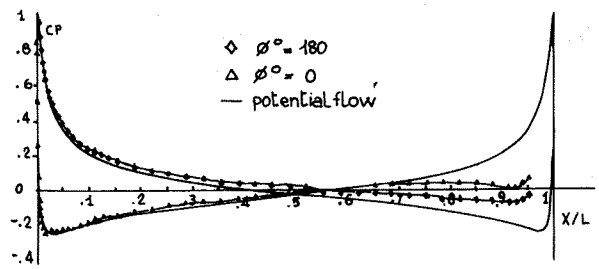

Fig.6c - Pressure coefficient distributions along the model for different angles Φ. $Re = 3 \times 10^6$, $\alpha = 14°$. Fixed transition, $(x/L)_{trans} = .20$

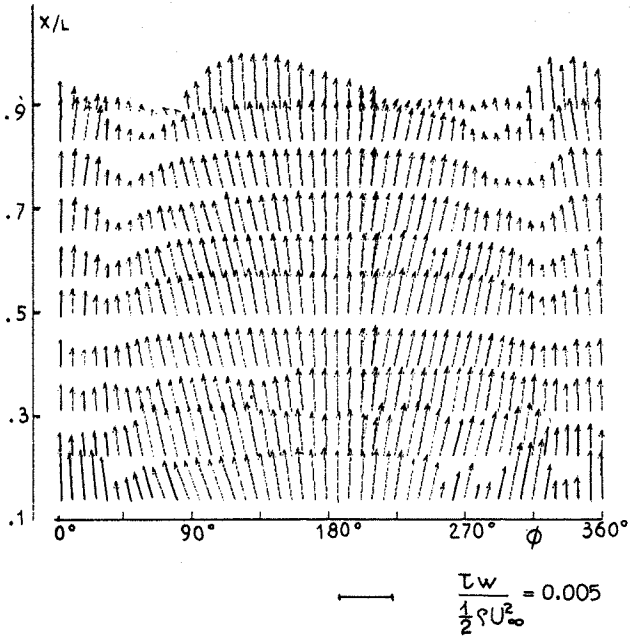

Fig.7 - Shear stress polar plot. $Re = 3 \times 10^6$, $\alpha = 14°$. Fixed transition, $(x/L)_{trans} = .20$

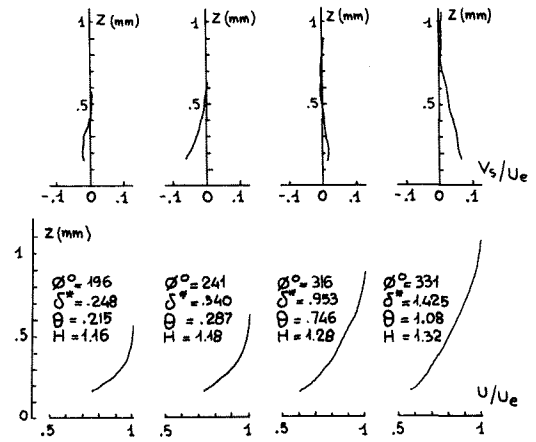

Fig.8 - Boundary layer total velocity U/Ue and cross velocity Vs/Ue profiles, for x/L = 0.309 and different values of Φ. $Re = 3 \times 10^6$, $\alpha = 14°$. Fixed transition, $(x/L)_{trans} = .20$

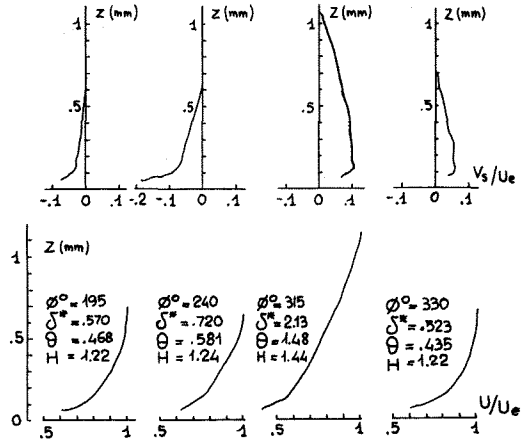

Fig.8 - Boundary layer total velocity U/Ue and cross velocity Vs/Ue profiles, for x/L = 0.652 and different values of Φ. $Re = 3 \times 10^6$, $\alpha = 14°$. Fixed transition, $(x/L)_{trans} = .20$

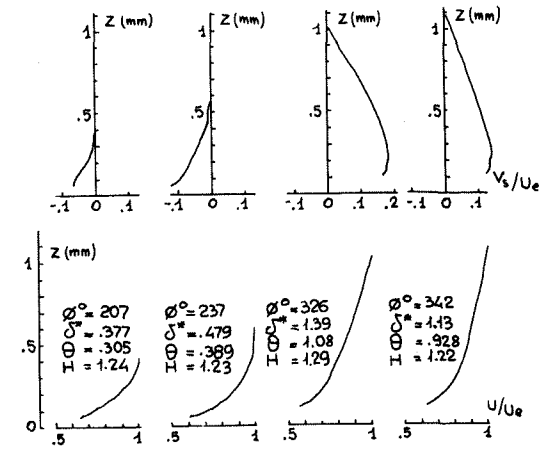

Fig.8 - Boundary layer total velocity U/Ue and cross velocity Vs/Ue profiles, for x/L = 0.493 and different values of Φ. $Re = 3 \times 10^6$, $\alpha = 14°$. Fixed transition, $(x/L)_{trans} = .20$

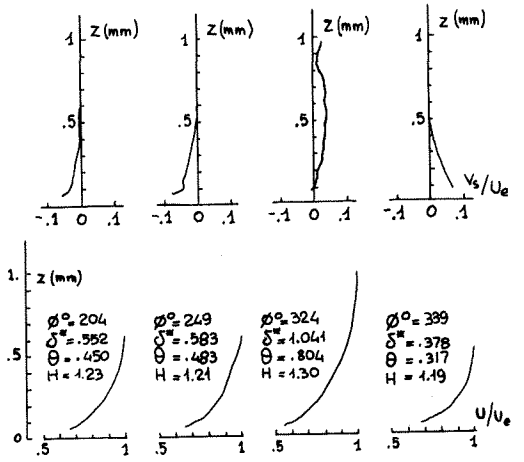

Fig.8 - Boundary layer total velocity U/Ue and cross velocity Vs/Ue profiles, for x/L = 0.738 and different values of Φ. $Re = 3 \times 10^6$, $\alpha = 14°$. Fixed transition, $(x/L)_{trans} = .20$

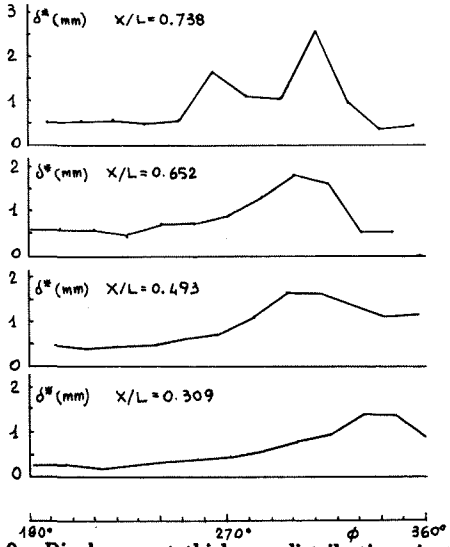

Fig.9 - Displacement thickness distributions in the circumferential direction and for different cross sections. $Re = 3 \times 10^6$, $\alpha = 14°$. Fixed transition, $(x/L)_{trans} = .20$

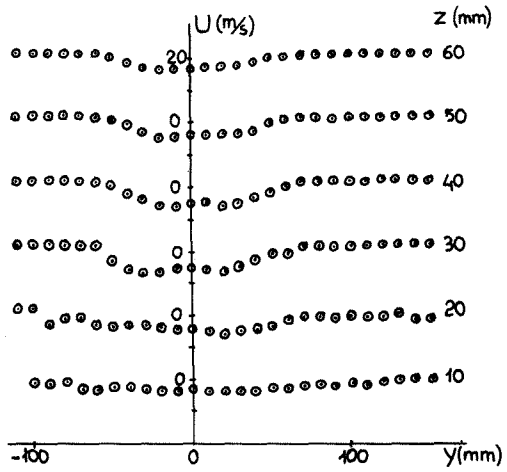

Fig.10a - Distribution of the longitudinal velocity in function of the lateral distance y, for different heights z above the model. x/2a = 0.480; ($V_\infty = 20m/s$); $\alpha = 30°$. Free transition. LDV measurements.

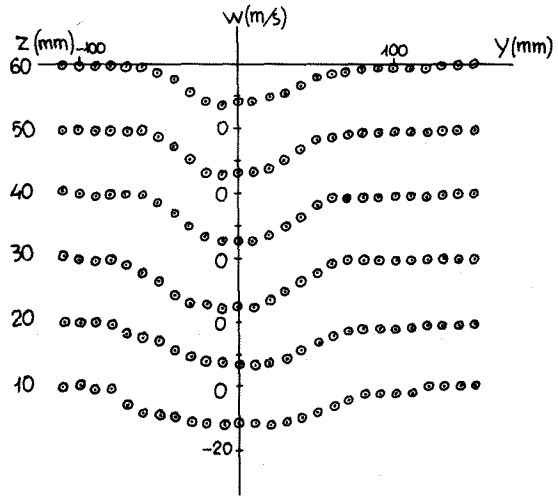

Fig.10b - Distribution of the vertical velocity in function of the lateral distance y, for different heights z above the model. x/2a = 0.480; ($V_\infty = 20m/s$); $\alpha = 30°$. Free transition. LDV measurements.

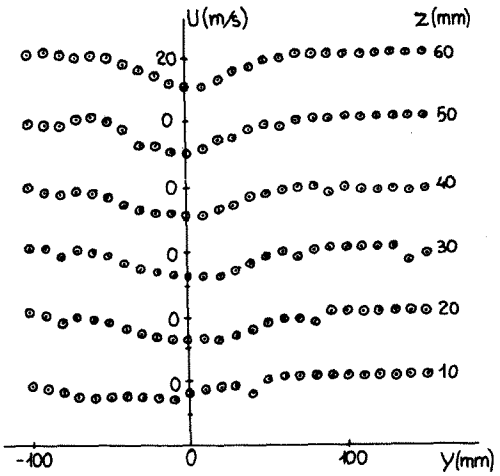

Fig.10a - Distribution of the longitudinal velocity in function of the lateral distance y, for different heights z above the model. x/2a = 0.652; ($V_\infty = 20m/s$); $\alpha = 30°$. Free transition. LDV measurements.

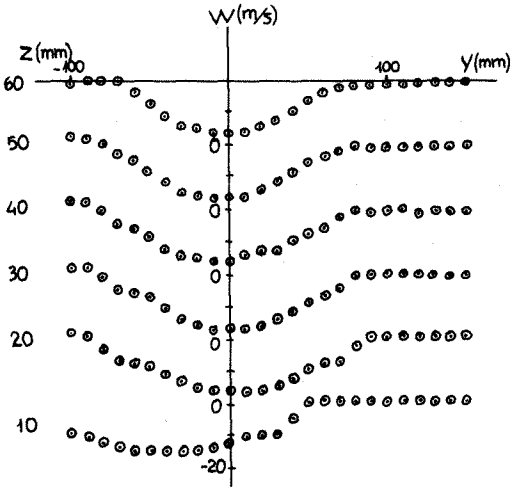

Fig.10b - Distribution of the vertical velocity in function of the lateral distance y, for different heights z above the model. x/2a = 0.652; ($V_\infty = 20m/s$); $\alpha = 30°$. Free transition. LDV measurements.